ISSN 0031-918X, The Physics of Metals and Metallography, 2013, Vol. 114, No. 6, pp. 514–520. © Pleiades Publishing, Ltd., 2013.
Original Russian Text © M.V. Ivchenko, V.G. Pushin, A.N. Uksusnikov, N. Wanderka, 2013, published in Fizika Metallov i Metallovedenie, 2013, Vol. 114, No. 6, pp. 561–568.

STRUCTURE, PHASE TRANSFORMATIONS, AND DIFFUSION

Microstructure Features of High-Entropy Equiatomic Cast AlCrFeCoNiCu Alloys

M. V. Ivchenko[a], V. G. Pushin[a, b], A. N. Uksusnikov[a], and N. Wanderka[c]

[a] *Institute of Metal Physics, Ural Branch, Russian Academy of Sciences, ul. S. Kovalevskoi 18, Ekaterinburg, 620990 Russia*
[b] *Yeltsin Ural Federal University, ul. Mira 19, Ekaterinburg, 620002 Russia*
[c] *Helmholtz-Zentrum Berlin for Materials and Energy, Hahn-Meitner-Platz 1, Berlin, 14109 Germany*
e-mail: MVIvchenko@yandex.ru

Received August 30, 2012; in final form December 11, 2012

Abstract—The structural and phase transformations that take place in the cast high-entropy equiatomic alloy AlCrFeCoNiCu after solidification, homogenizing heat treatment, and cooling have been studied. Analytical transmission microscopy, scanning electron microscopy, X-ray energy dispersive spectroscopy, and X-ray diffraction analysis were used to conduct the studies. The elastic modulus, nano-, and microhardness have been measured. The alloy decomposition has been found to occur with the precipitation of no less than six nanoscale phases with different morphologies, structures ($A2$, $B2$, $L1_2$), and chemical compositions. All the nanophases are multicomponent solid solutions enriched with several elements, which indicates the pronounced elemental and phase nanomodulation over the alloy volume.

Keywords: high-entropy equiatomic alloy, mixing entropy, spinodal decomposition, structural and phase transformations, nanophases, chemical composition

DOI: 10.1134/S0031918X13060069

INTRODUCTION

Despite the very long period of the development of metal science as a practical and scientific field of human activity, one and sometimes two or three metals serve as the base components for the vast majority of studied and, in particular, practically used metallic materials. Generally speaking, there are only two or three dozen frequently used conventional metals, including iron, aluminum, copper, precious metals, nickel, titanium, tin, lead, zinc, magnesium, niobium, zirconium, beryllium, and refractory, radioactive, and other metals [1–7].

In the second half of the 20th century, the natural needs of developing industry for various structural and functional materials had stimulated the emergence of new technologies to create high-alloy steels and alloys. This increased the number of alloying elements, as well as their fraction in the total material mass. For instance, some primarily corrosion-resistant, heat-resistant, and high-strength steels and alloys already contain four or five controllable alloying elements up to 30–40% in weight; high-strength aluminum alloys include three or four elements up to 10–15% in weight; and brass and bronze, up to 40 and 15%, respectively [1–9].

In the 1960s, intermetallics, a broad class of compounds that consist of original metal elements, were studied. The intermetallic compounds atomically ordered to form different types ($A15$, $B2$, $C15$, $D0_3$, $L1_0$, $L1_2$, $L2_1$, etc.) have unique functional properties, including superconductivity (Nb_3Sn, V_3Ga); magnetism (Fe, Ni, and Co compounds); heat resistance (NiAl, CoAl, CoNiAl), heat stability (Ni_3Al, Ti_3Al, TiAl); and shape memory effect and properties controlled by heat, strain, or magnetization (TiNi, Ni_2MnGa, etc.) [6–13].

However, the application of many of these alloys and intermetallic compounds is significantly limited because of their unacceptably low values of several service properties. Therefore, the next important step, aimed primarily at improving their structural, functional, and technological characteristics, was associated with micro and macro alloying with third, fourth, and fifth element, the development of new modern strengthening and plasticizing technologies for synthesis and subsequent processing of poly and single crystals, and the modification and arrangement of their micro- and submicrocrystalline structures [4–13].

Thus, the historical development of science and technology has predetermined the appearance of first studies on the formation and research of so-called high-entropy metal alloys containing already from five to six main elements, each with a concentration of 5–35%, at the beginning of the 21st century [14]. In particular, these alloys include AlCoCrCuFeNi, CoCrCuFeNiTi, and CuNiAlCoCrFeSi [14–18]. Along with characteristics typical of metal alloys, high-entropy alloys exhibit unique and unusual properties typical of, e.g., metalloceramics, including high hardness, high resistance to softening at high temperatures, a positive coefficient of temperature hardening, and high strength properties at ele-

Crystal structure and chemical composition (at %) of the cast alloy AlCrFeCoNiCu (uncertainty in chemical composition measurement, of ±2% and the lattice parameter measurement, of ±0.005 nm)

Chemical composition	Method and identified region	Structure and lattice parameter, nm	Al	Cr	Fe	Co	Ni	Cu
AlCrFeCoNiCu	Nominal melt content	–	16.6	16.6	16.6	16.6	16.6	16.6
Cu–Ni–Al	TEM (D), dendrite	*B*2; 0.288	5	1	2	2	5	85
Cr–Fe–Co	TEM (B), dendrite	*A*2; 0.288	2	43	30	20	5	0
Ni–Al–Co–Fe	TEM (A, C), dendrite	*B*2; 0.288	20	6	14	20	30	10
Cu–Ni–Co–Al	TEM (E), dendrite	$L1_2$; 0.364	8	3	7	9	15	58
Cu–Ni–Al–Fe–Co–Cr	TEM (F), interdendritic region	$L1_2$; 0.358	7	1	3	3	9	77
Al–Cr–Fe–Co–Ni–Cu	SEM, dendrite	*B*2 (*A*2, $L1_2$)	17	21	18	17	16	11
Cu–Ni–Al–Fe–Co–Cr	SEM, interdendritic region	*A*1 ($L1_2$)	12	3	5	5	12	63
Al–Cr–Fe–Co–Ni–Cu [16]	SEM, dendrite	bcc	15	25	21	20	12	7
Cu–Ni–Al–Fe–Co–Cr [16]	SEM, interdendritic region	fcc/bcc	14	7	8	9	12	50

vated temperatures, as well as an attractive corrosion resistance and other properties [14–18].

The microstructure, chemical and phase composition of the initial multicomponent equiatomic cast alloy AlCrFeCoNiCu have been studied in this paper. Bcc and fcc phases with dendritic microstructure are known to form in the alloys of this system. The morphology and phase composition of the microstructure depends on the chemical composition, in particular on the aluminum content [14–16]. The equiatomic alloy exhibited modulated bcc lamellar phases with a *B*2 atomic ordered structure and *A*2 disordered one resulted from spinodal decomposition in the dendritic matrix [15, 16]. It is also assumed that, by contrast, a two-phase mixture of fcc and bcc phases enriched with copper [15, 16] was formed as a result of eutectic reaction within interdendritic regions. However, the results obtained in [14–18] are quite ambiguous and often contradictory. With allowance for these facts, in our work, we paid particular attention to the study of thin nanostructured and nanophase structure features of the cast alloy using primarily analytical methods of modern transmission and scanning electron microscopy.

EXPERIMENTAL

For the study, the ingot of high-entropy equiatomic alloy AlCrFeCoNiCu, consisting of six high-purity components (99.999%), 20 mm in diameter was melted in the atmosphere of purified argon. The ingot was remelted five times to improve chemical homogeneity, then homogenized for a long time in a vacuum furnace at 1000°C (24 h) and slowly cooled at a rate of 10 K/s. The ingot was cut into thin, platelike samples to be studied. The structure of the samples was examined by analytical electron microscopy (AEM), transmission (TEM) and scanning electron microscopy (SEM), as well as by X-ray diffraction analysis (XRDA). The electron-microscopic investigations were performed using a Philips CM 30 Supertwin microscope (at an accelerating voltage of 300 kV) and a Quanta 200-Pegasus instrument (at an accelerating voltage of 30 kV). The local chemical analysis was conducted using X-ray energy dispersive EDAX spectrometers with which these microscopes were equipped. The cross section of the electron beam was ~10 nm for TEM and ~400 nm for SEM studies. XRDA was carried out on Bruker AXS D8 and DRON-3M X-ray diffractometers for the investigation of mechanically and electrolytically polished samples, by the θ/2θ method in monochromatized Cu *K*α radiation. The hardness was measured by the standard microhardness tester. The hardness and modulus of elasticity were also determined by the nanoindentation method on the Fischer Picadentor NM500 tester using a tetrahedral diamond pyramid with an angle of 136° between opposite faces under a load of 300 mN for 20 s.

RESULTS

The X-ray diffraction study of the cast alloy AlCrFeCoNiCu has shown that it is in the multiphase structural state and does contain the bcc and fcc phases. The interpretations of the most intense Bragg reflections allowed us to identify a bcc phase with the parameter $a_{bcc} = (0.288 \pm 0.005)$ nm as the main matrix phase. In addition, there were weaker and broadened reflections from two fcc phases with parameters $a_{fcc1} = (0.362 \pm 0.005)$ nm and $a_{fcc2} = (0.359 \pm 0.005)$ nm, which were observed in the form of asymmetric doublets closely located. The reflections of the second fcc phase were somewhat more pronounced. On the whole, the data are consistent with those previously published in [14–16, 18].

The chemical composition of the alloy was defined by means of SEM analysis using X-ray energy dispersive spectroscopy (EDS) in local volumes with sizes of a few tenths of micrometers. The distribution of chemical elements over the alloy volume was found to be significantly nonuniform (see, table). Taking into consideration the published data and our SEM and TEM

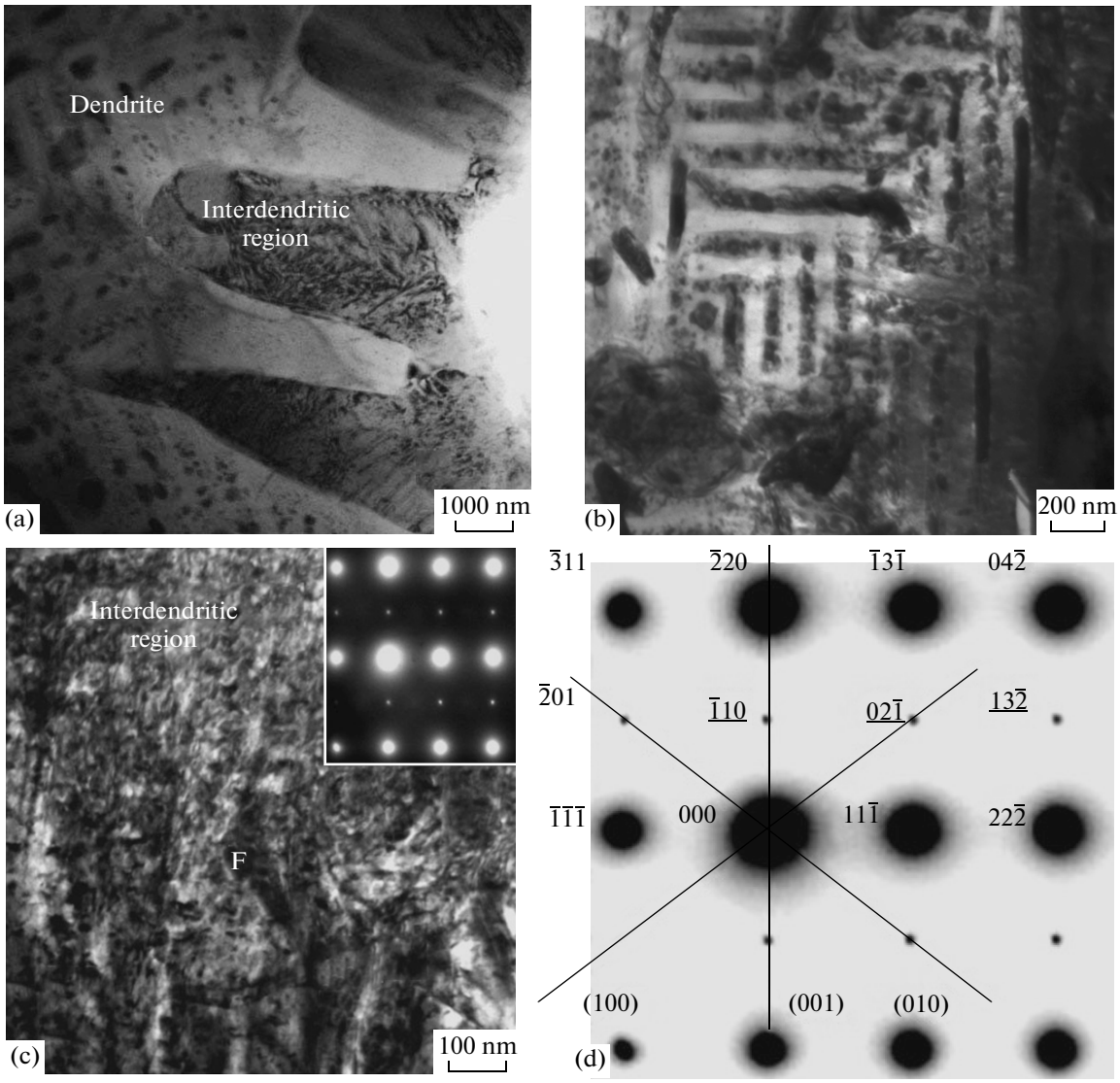

Fig. 1. (a), (b) Bright- and (c) dark-field images of the interdendritic microstructure of the cast AlCrFeCoNiCu alloy. (d) Electron diffraction pattern scheme in the inset; the solid lines indicate {100} trace planes, along which the images of α_1 habitus of Widmanstätten plates are located.

results, it can be concluded that, in the cast alloy, the formation of a microstructure with the typical morphology of dendrites and interdendritic joints and their subsequent degradation occurred in the process of phase separation (Fig. 1a).

It follows from a TEM analysis of fringe-contrast images, which illustrates the Widmanstätten lamellar precipitates with a thickness of 50–60 nm, a length of 500 nm, and orientation along habit planes that are close to $\{100\}_{fcc}$, that interdendritic regions are not single-phase (Figs. 1a–1c). Based on the interpretation of the corresponding electron diffraction pattern (inset in Fig. 1c) with the $\langle 112\rangle_{fcc}$ zone axis of reflecting planes, the interdendritic region generally has an fcc structure with a parameter of about 0.358 nm (in agreement with X-ray data of the second fcc phase). The presence of weaker superstructure reflections of the 110 and 120 types in electron diffraction patterns (Figs. 1c, 1d) indicates the existence of an atomic $L1_2$ order. However, both the presence of contrast bands in bright- and dark-field images and their fragmented nonuniform patterns (Figs. 1b, 1c) make it impossible to draw an unambiguous conclusion that the entire interdendritic region is of the same atomic ordering. Thus, based on a comparison of the SEM data on the elemental X-ray analysis of large interdendritic regions (~400 nm in cross-section) and TEM data on the local analysis, carried out with the use of EDS of volumes ~10 nm in cross-section, we have arrived to the conclusion that local differences in chemical composition are significant (see, table). It can be concluded that the precipitates designated by us

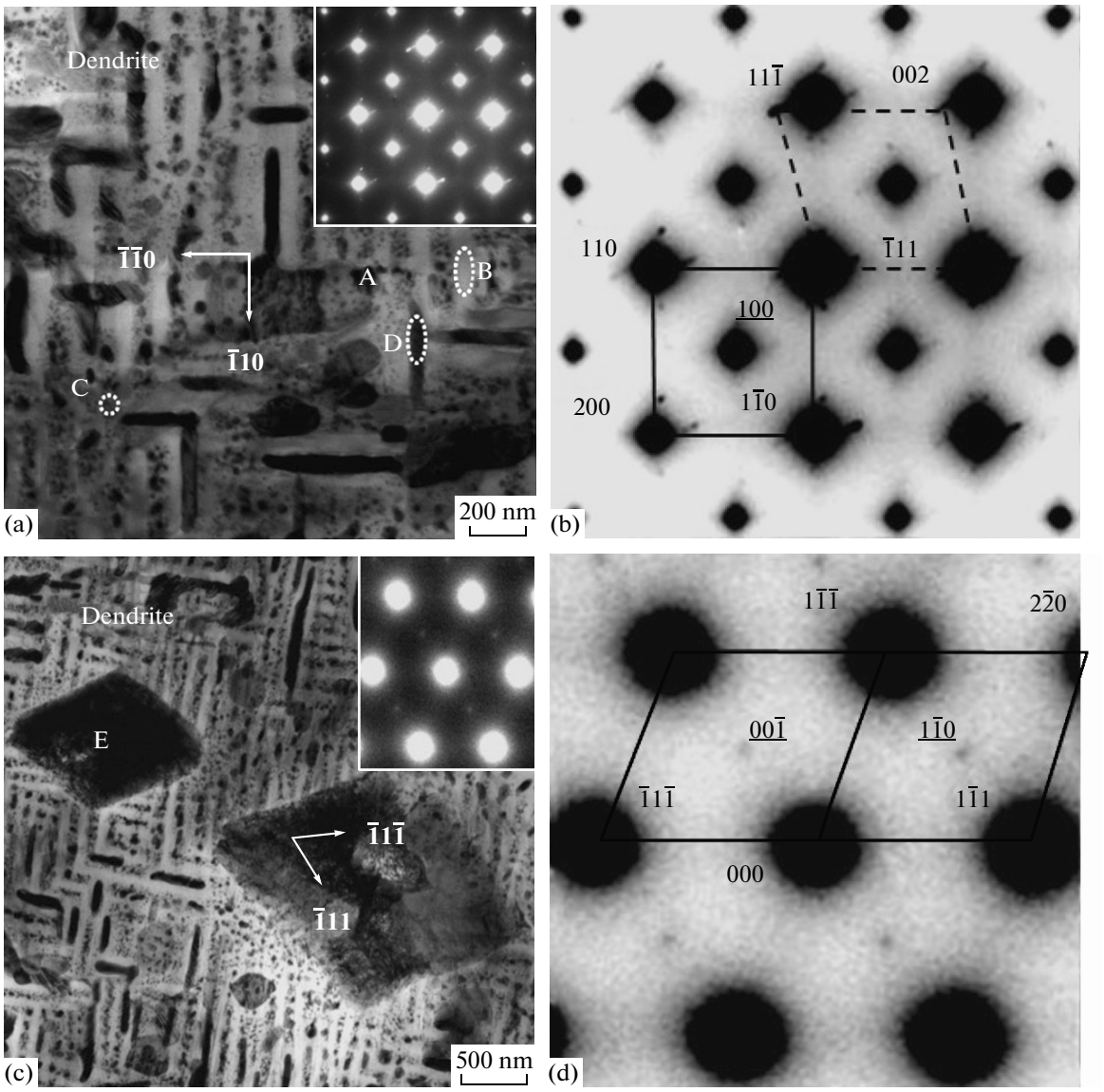

Fig. 2. (a), (c) Bright-field images of the dendritic microstructure with the corresponding electron diffraction patterns (in insets) and (b), (d) the schemes of their interpretations; (b) axis zones: (solid line) $\langle 001\rangle_{B2}$ and (dash line) $\langle 1\,10\rangle_{L1_2}$.

as α_1 and copper-enriched phases (up to 77 at % Cu), compared to the surrounding interdendritic region (63 at % Cu) demonstrate its isomorphic decomposition. We cannot exclude the presence of some amount of the bcc phase of eutectic nature in it [15, 16].

Figure 2 shows characteristic electron microscopic images of the main dendritic structure actually prevailing in the cast alloy volume. Corresponding electron diffraction patterns are demonstrated in the insets in Fig. 2a and 2c and schemes of their interpretations in Figs. 2b and 2c. The main feature of the dendrites is the presence of alternating (if we judge based on the uniform contrast in TEM images) Widmanstätten lamellar precipitates 40–50 nm thick and 500–600 nm long, which, however, are oriented along the habit $\{110\}_{\text{bcc}}$ planes. This was evidenced by the trace analysis of the corresponding diffraction pattern shown in the inset of Fig. 2a, with the $\langle 001\rangle_{\text{bcc}}$ zone axis of the reflecting planes. Based on the measurements, the bcc lattice parameter is close to 0.288 nm. Together with structural reflections, bright superstructure reflections of the 100_{B2} type are observed, as well as diffuse scattering in the form of modulated strikes and satellites near the reflections and along the directions $\langle 110\rangle_{B2}$ of the reciprocal lattice in the electron diffraction pattern. This fact proves the presence of atomic ordering of the *B*2-bcc type in the Widmanstätten lamella. The electron diffraction pattern also exhibits four grids of less pronounced fcc reflections with zone axis $\langle 110\rangle_{\text{fcc}}$ (scheme in Fig. 2b). In addition to bright and dark

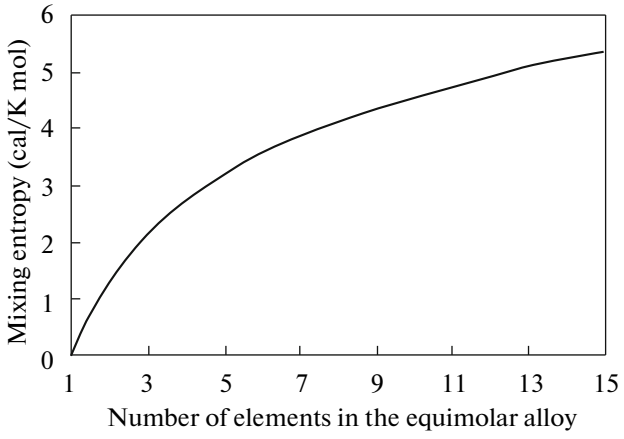

Fig. 3. Dependence of the mixing entropy on the number of chemical elements in disordered alloy [14].

bands of uniform contrast, the position of which are indicated by letters D and B in Fig. 2a, the TEM images of dendrites illustrate darker contrasts of spherical particles with sizes of 10–30 nm, indicated by A and C, which are also visible in the *B*2 superstructure reflections of a type 100. Often, their location was not accidental and they accumulated layers generally parallel to the Widmanstätten lamellae (Figs. 2a, 2c). Finally, Fig. 2c also shows a coarser cubic-rhomb-shaped precipitates of micron sizes in the dendrites, indicated by E. These precipitates have atomic-ordered $L1_2$ structures, which can be seen from the electron diffraction pattern in the inset to Fig. 2c and corresponding interpretation in Fig. 2d. The $L1_2$ lattice parameter is close to 0.363 nm, which corresponds to the parameter of the first fcc phase revealed by X-ray diffraction ($a_{fcc} = 0.362$ nm). We may conclude that the complex electron diffraction pattern in Fig. 2a with weak additional fcc-phase reflections (Fig. 2b) corresponds to the dendritic regions with this phase. Orientation relations between bcc and fcc phases determined by analyzing this electron diffraction pattern are close to $\{001\}_{B2} \parallel \{110\}_{L1_2}$ and $\langle 110\rangle_{B2} \parallel \langle 111\rangle_{L1_2}$.

TEM data on the elemental composition of the phase particles precipitated in dendrites obtained using X-ray EDS with a locality of the analyzed volume of ~10 nm in the lateral section are listed in the table. This table also contains our own and published data on the average chemical composition of dendrites in the alloy under study. These data were measured in SEM studies using a probe 0.4–0.5 μm wide (the uncertainty in measurement is no less than 2–3%; therefore, our and published data in the table are expressed in round whole numbers). When analyzing the results, it should be noted that four multicomponent solid solution based on cubic phases *A*2, *B*2, and $L1_2$ have been found with significant differences in chemical compositions. Lamellar nanoparticles (indicated by D) of a darker contrast are identified as the *B*2 phase enriched in Cu (up to 85 at %), Ni, and Al (up to 5 at %) and contain three other elements (Fe, Co, Cr) in amounts less than 5 at %. Lamellae that are parallel to the previously described particles and brighter regions (B) correspond to the disordered bcc *A*2 phase. On the contrary, they are enriched in Cr (up to 43 at %), Fe (up to 30 at %), and Co (up to 20 at %), including no more than 5 and 2 at % Ni and Al, respectively, with little Cu. The spherical dispersed *B*2-nanoparticles (A, C) seem to belong to the same *B*2 phase based on the system Ni–Al–Co and, being in *B*2 solid solution, they contain Ni (up to 30–31 at %), Al (up to 20–26 at %), Co (up to 18–20 at %), Fe (12–14 at %), Cu (up to 10 at %), and Cr (6.3 at %). Finally, the copper-rich micron particles of the atomic-ordered $L1_2$ phase (indicated by E in Fig. 2c) include Cu (up to 60 at %); Ni (up to 15 at %); and Co, Al, and Fe (up to 7–9 at %), as well as Cr (up to 3 at %). The average chemical composition that is integrated over the volume of dendrites is markedly different from the nominal one (16.6 at % of each element). In general, these integrated data are in quite good agreement, considering the different synthesis conditions and heat treatment, with the known published data [15, 16, 18].

The mean values of the elastic modulus (182 GPa) and hardness (534 *HV*) obtained by nanoindention are fairly high, and the nanohardness is close to our measurements of microhardness (500 *HV*) and to known published data [16].

DISCUSSION

As has already been mentioned, the studied cast metal alloy belongs to high-entropy alloys. Their distinctive feature is the solidification-induced formation of phases based on multicomponent solid solutions, provided that equiatomic multicomponent (4–5 or more metals) alloying is performed [14], and they are expected to have simple bcc or fcc structures and provide, even at high temperatures, significant precipitation hardening and thermal stability of the microstructure and properties. In this case, the alloys really must have a number of attractive physical and mechanical, chemical, and service properties [14]. In the thermodynamic sense, the main factor responsible for the formation of metallic alloys based on multicomponent cubic solid solutions is the entropy of mixing. Its dependence on the number of alloying elements in the equiatomic alloys completely disordered is shown in Fig. 3 [14]. It is believed that a significant increase in the entropy is accompanied by an adequate reduction in the free (or Gibbs) energy of the system with an increase in the number of components in the equiatomic alloys. This stabilizes nonequilibrium solid-solution state and makes it competitive with softening processes in the alloy.

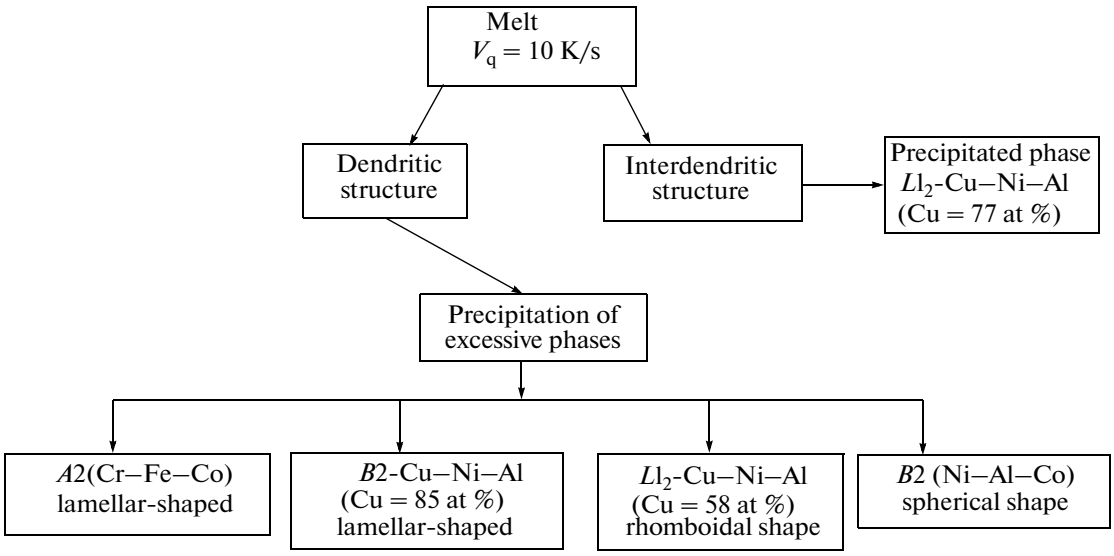

Fig. 4. Scheme of decomposition of cast AlCrFeCoNiCu alloy after homogenization and cooling to room temperature.

When discussing the experimental results taking into consideration all mentioned above, it is important to note that a highly unstable structural phase state is retained even in the cast high-entropy alloy. The main structural features include the following: the presence of a small number of multicomponent crystalline phases rather uniformly distributed in dendrites and interdendritic regions; the presence of simple cubic phases, which are both disordered ($A2$) and atomic-$B2$ and $L1_2$ ordered; the nanoscale of the phases and the prevalence of isotropic or intermediate-anisotropic morphological forms due to block-discretization structure and uniform spatial arrangement of all nanophases; the nanomodulated distribution of chemical composition and nanophases (and as expected in a number of papers, spinodal phase separation of solid-solution initial phases); the implementation of the rational dimension-orientation relationships between phases and, obviously, the implementation of their interfacial conjugation of mostly coherent nature.

Thus, it should be emphasized that the alloy did undergo decomposition during slow solidification and subsequent heat treatment. This process was accompanied by the formation of the four phases in dendrites and the wo phases, namely, those enriched in and depleted of copper, in the interdendritic regions (Fig. 4). However, their number is much less than the maximum possible number under equilibrium conditions according to the Gibbs phase rule [14].

When considering these results, we must discuss the unique experiments previously published in [18]. The same cast alloy was used to study at atomic resolution the local distribution of the chemical elements, using a three-dimensional Cameca Atom Probe (3D-AP) scanner. In addition to the above results on the phase composition of the alloy, the 3D-AP tomography method was used to reveal the periodic concentration fluctuations and segregations of chemical elements (with sizes of one to dozens of nanometers) within the dendritic matrix. We identified a whole number of different clusters with different elements, i.e., Cu (up to 90 at %)–Ni (4–5 at %)–Al (up to 4–5 at %); Cr (up to 40 at %)–Fe (up to 31 at %)–Co (up to 19 at %); and clusters based on Al–Ni–Co, Al–Ni–Fe, Ni–Cr–Fe, and Ni–Cr–Fe–Co. It is obvious that the detected concentrations of 3D distributions are associated with the detected nanophases and demonstrate a highly complex and nontrivial nature in high-entropy alloys.

CONCLUSIONS

Based on the results of the present study and already known data, the following conclusions can be drawn:

(1) In the cast multicomponent high-entropy equiatomic AlCrFeCoNiCu alloy, solidification, followed by homogenization and cooling, has led to the decomposition with the precipitation of at least six phases that have different morphologies, structure types ($A2$, $B2$, and $L1_2$), and chemical compositions within the formed dendritic and interdendritic regions.

(2) The precipitates are characterized by nanoscale sizes and mostly equiaxed or lamellar shapes. They are uniformly distributed between themselves and over the alloy volume. They possess size-orientated and coherent relationships with the matrix both in dendrites and interdendritic regions.

(3) All nanophases are multicomponent solid solutions enriched in several elements, which leads to the pronounced modulation of the elemental and phase compositions over the alloy volume. This is well con-

firmed by the data obtained by the three-dimensional atomic alloy scanning. These data has shown that the distribution of all the chemical elements is characterized by their consistent periodic nanoscale modulation [18].

ACKNOWLEDGMENTS

This work was supported in part by the Presidium of the Russian Academy of Sciences, project no. 12-P-2-1060; and by the Ural Branch of Russian Academy of Sciences project no. 12-M-235-2063.

REFERENCES

1. M. L. Bernshtein, *Thermomechanical Treatment of Alloys*, in 2 vols. (Metallurgiya, Moscow, 1968) [in Russian].
2. B. A. Kolachev, V. A. Livanov, and V. I. Elagin, *Metal Science and Heat Treatment of Non-Ferrous Metals and Alloys* (Metallurgiya, Moscow, 1972) [in Russian].
3. G. V. Kurdyumov, L. M. Utevskii, and R. I. Entin, *Transformations in Iron and Steel* (Nauka, Moscow, 1977) [in Russian].
4. I. I. Fridlyander, *Aluminum Deformable Structural Alloys* (Metallurgiya, Moscow, 1979) [in Russian].
5. Glezer, A.M. and Molotilov, V.V., *Ordering and Deformation of Iron Alloys* (Metallurgiya, Moscow, 1984) [in Russian].
6. V. N. Khachin, V. G. Pushin, and V. V. Kondrat'ev, *Titanium Nickelide: Strtucture and Properties* (Nauka, Moscow, 1992) [in Russian].
7. V. G. Pushin, V. V. Kondrat'ev, and V. N. Khachin, *Pretransition Phenomena and Martensitic Transformations* (Ural. Otd. Ross. Akad. Nauk, Ekaterinburg, 1998) [in Russian].
8. E. N. Kablov and E. R. Golubovskii, *Heat Resistance of Nickel Alloys* (Mashinostroenie, Moscow, 1998) [in Russian].
9. "To 70th anniversary of VIAM: A special issue," Metal Sci. Heat Treat., No. 7 (2002).
10. B. A. Greenberg and M. A. Ivanov, *Ni_3Al and TiAl Intermetallic Compounds: Microstructure and Deformation Behavior* (Ural. Otd. Ross. Akad. Nauk, Ekaterinburg, 2002) [in Russian].
11. V. G. Pushin, S. D. Prokoshkin, R. Z. Valiev, V. Brailovskii, E. Z. Valiev, A. E. Volkov, A. M. Glezer, S. V. Dobatrin, E. F. Dudarev, V. T. Zhu, Yu. G. Zainulin, Yu. R. Kolobov, V.V. Kondratiev, A. V. Korolev, A. I. Korshunov, N. I. Kourov, N. V. Kudrevatykh, A. I. Lotkov, L. L. Meisner, A. A. Popov, N. N. Popov, A. I. Razov, M. A. Khusainov, Yu. I. Chumlyakov, S. V. Andreev, A. A. Baturin, S. P. Belyaev, V. N. Grishkov, D. V. Gunderov, A. P. Dyupin, K. V. Ivanov, V. I. Itin, M. K. Kasymov, O. A. Kashin, I. V. Kireeva, A. I. Kozlov, T. E. Kuntsevich, N. N. Kuranova, N. Yu. Pushina, E. P. Ryklina, A. N. Uksusnikov, I. Yu. Khmelevskaya, A. V. Shelyakov, V. Ya. Shklover, E. V. Shorokhov, and L. I. Yurchenko, *Titanium Nickelide Alloys with Shape Memory. Ch. I. Structure, Phase Transformations and Properties* (Ural. Otd. Ross. Akad. Nauk, Ekaterinburg, 2006) [in Russian].
12. V. G. Pushin, "Alloys with a thermomechanical memory: Structure, properties, and application," Phys. Met. Metallogr. **90** (Suppl. 1), S68–S95 (2000).
13. V. Brailovski, I. Yu. Khmelevskaya, S. D. Prokoshkin, V. G. Pushin, E. P. Ryklina, and R. Z. Valiev, "Foundations of heat and thermomechanical treatments and their effect on the structure and properties of titanium nickelide-based alloys," Phys. Met. Metallogr. **97** (Suppl.1), S3–S55 (2004).
14. J. W. Yeh, Y. L. Chen, S. J. Lin, and S. K. Chen, "High-entropy alloys—A new era of exploitation," Mater. Sci. Forum **560**, 1–9 (2007).
15. C. J. Tong, Y. L. Chen, S. K. Chen, J. W. Yeh, T. T. Shun, C. H. Tsau, S. J. Lin, and S. Y. Chang, "Microstructure characterization of Al_xCoCrCuFeNi high-entropy alloy system with multiprincipal elements," Metall. Mater. Trans. A **36 A**, 881–893 (2005).
16. C. C. Tung, J. W. Yeh, T. T. Shun, S. K. Chen, Y. S. Huang, and H. C. Chen, "On the elemental effect of AlCoArCuFeNi high-entropy alloy system," Mater. Lett. **61**, 1–5 (2007).
17. X. F. Wang, Y. Zhang, Y. Qiao, and G. L. Chen, "Novel microstructure and properties of multicomponent CoCrCuFeNiTi$_x$ alloys," Intermetallics **15**, 357–362 (2007).
18. S. Singh, N. Wanderka, B. S. Murty, U. Glatzel, and J. Banhart, "Decomposition in multi-component AlCoCrCuFeNi high-entropy alloy," Acta Mater. **59**, 182–190 (2011).

Translated by T. Gapontseva